

Large muon ($g - 2$) with TeV-scale SUSY masses for $\tan \beta \rightarrow \infty$

Markus Bach^a, Jae-hyeon Park^b, Dominik Stöckinger^a,
Hyejung Stöckinger-Kim^a

^a *Institut für Kern- und Teilchenphysik, TU Dresden, 01069 Dresden, Germany*

^b *Departament de Física Teòrica and IFIC, Universitat de València-CSIC, 46100, Burjassot, Spain*

Abstract

The muon anomalous magnetic moment a_μ is investigated in the MSSM for $\tan \beta \rightarrow \infty$. This is an attractive example of radiative muon mass generation with completely different qualitative parameter dependence compared to the MSSM with the usual, finite $\tan \beta$. The observed, positive difference between the experimental and Standard Model value can only be explained if there are mass splittings, such that bino contributions dominate over wino ones. The two most promising cases are characterized either by large Higgsino mass μ or by large left-handed smuon mass m_L . The required mass splittings and the resulting a_μ^{SUSY} are studied in detail. It is shown that the current discrepancy in a_μ can be explained even in cases where all SUSY masses are at the TeV scale. The paper also presents useful analytical formulas, approximations for limiting cases, and benchmark points.

1 Introduction

The muon anomalous magnetic moment $a_\mu = (g - 2)_\mu/2$ provides a tantalizing hint for physics beyond the Standard Model (SM). The current discrepancy between experiment and theory¹ is

$$a_\mu^{\text{exp}} - a_\mu^{\text{SM}} = (28.7 \pm 8.0) \times 10^{-10}. \quad (1)$$

It can be explained by a variety of new physics models below or at the TeV scale. Generally, the new physics contributions a_μ^{NP} are strongly correlated with the loop contributions to the muon mass, δm_μ^{NP} , and they are suppressed by two powers of the typical new physics mass scale M_{NP} [5, 18]. This relation can be written as

$$a_\mu^{\text{NP}} = C_{\text{NP}} \frac{m_\mu^2}{M_{\text{NP}}^2}, \quad (2)$$

where $C_{\text{NP}} = \mathcal{O}(\delta m_\mu^{\text{NP}}/m_\mu)$ is given by the model-dependent relative contribution to the muon mass.

Of special interest are, therefore, models of radiative muon mass generation: in these models, δm_μ^{NP} amounts to the entire physical muon mass and $C_{\text{NP}} = \mathcal{O}(1)$. Excluding fine-tuning in the muon mass, these models yield the largest a_μ^{NP} , compared to other ones with the same new physics scale M_{NP} . As the estimate $a_\mu^{\text{NP}} = \mathcal{O}(m_\mu^2/M_{\text{NP}}^2)$ holds, the observed deviation can in principle be explained by a new physics scale of the order 2 TeV.

The general idea of radiative muon mass generation can be realized in the renormalizable and calculable framework of the minimal supersymmetric standard model (MSSM). As discussed below in Sec. 2 there are two distinct possibilities, one of which has already been studied in Refs. [19–21]. The possibility considered in the present paper is the limit

$$\tan \beta \equiv \frac{v_u}{v_d} \rightarrow \infty \quad (3)$$

with the up- and down-type Higgs vacuum expectation values $v_{u,d}$. In this limit v_d , the muon mass, and all other down-type lepton and quark masses vanish at tree level. The masses arise from finite loop diagrams generating non-holomorphic couplings of down-type fermions to the “wrong” Higgs doublet H_u . These loop diagrams are also important for finite $\tan \beta$, and they have been discussed extensively in the literature, often in the context of B -physics [22], but also in the

¹ The experimental result has been obtained at BNL [1]; a fourfold improvement in precision is expected from the new experiments [2, 3]. For reviews of the theory prediction see Refs. [4, 5]; recent theory progress has been achieved on the QED [6, 7], electroweak [8], and hadronic contributions [9–13]; for specific reviews of the hadronic light-by-light contributions and expected future improvements see [14–17]. The value quoted in the text is based on the hadronic contributions from Ref. [9].

context of the muon magnetic moment [23]. Because of these loop diagrams, the limit $\tan\beta \rightarrow \infty$ exists and is phenomenologically viable [24, 25].

We will show in this paper that a_μ behaves very differently for $\tan\beta \rightarrow \infty$, and existing phenomenological analyses of a_μ in the MSSM (for reviews see [26–28]; recent works are [29–42]) do not apply. The MSSM in this limit is also no special case of the model-independent analysis of Ref. [43], where simplified models with only two relevant particle masses have been considered. We will see that all cases of interest involve at least three relevant masses at the TeV scale.

Considering a_μ in the MSSM for $\tan\beta \rightarrow \infty$ is interesting for two reasons. On the one hand, it is a calculable realization of the general idea of radiative muon mass generation, and the results can be indicative of the more general situation. On the other hand, it opens up an area of supersymmetry (SUSY) parameter space where a_μ behaves qualitatively very differently from the standard MSSM case (with moderate $\tan\beta$): in particular large a_μ is compatible with very heavy SUSY particles.

We now give a brief preview of the MSSM limit $\tan\beta \rightarrow \infty$ to set the stage for the remainder of the paper. In the simple case that all relevant SUSY masses are equal to M_{SUSY} and $\tan\beta$ is moderate, the SUSY contribution to a_μ is approximately given by the one-loop diagrams as

$$a_\mu^{\text{SUSY,1L}} \approx 13 \times 10^{-10} \text{sign}(\mu) \tan\beta \left(\frac{100 \text{ GeV}}{M_{\text{SUSY}}} \right)^2. \quad (4)$$

For large $\tan\beta$ it has already been shown in Ref. [23] that higher-order terms leading in $\tan\beta$ can become important and change the linear dependence. These higher-order terms can be resummed as

$$a_\mu^{\text{SUSY}} = \frac{a_\mu^{\text{SUSY,1L}}}{1 + \Delta_\mu}, \quad (5)$$

where, still in the case of equal SUSY masses, the self-energy leads to

$$\Delta_\mu \approx -0.0018 \text{sign}(\mu) \tan\beta. \quad (6)$$

Hence, in the desired limit of infinite $\tan\beta$ the SUSY contribution becomes

$$a_\mu^{\text{SUSY}} = \lim_{\tan\beta \rightarrow \infty} \frac{a_\mu^{\text{SUSY,1L}}}{\Delta_\mu} \approx -72 \times 10^{-10} \left(\frac{1 \text{ TeV}}{M_{\text{SUSY}}} \right)^2, \quad (7)$$

demonstrating that the magnitude of the contribution is very large, even for M_{SUSY} in the multi-TeV range. The proportionality to $\tan\beta$ has been replaced by a constant behaviour, and the dependence on $\text{sign}(\mu)$ has disappeared. However, the sign is predicted to be wrong, so such a scenario with infinite $\tan\beta$ and equal SUSY masses is definitely excluded.

If the SUSY masses are not all equal, the above approximations do not apply, and in the remainder of the paper we will give a full investigation of the five-dimensional parameter space. In particular we will characterize the regions that lead to a positive SUSY contribution to a_μ , which agrees with the observed deviation.

In Sec. 2 we define the model, provide analytical results and useful approximation formulas, and briefly review constraints from other sectors. Comprehensive numerical analyses and their physical interpretation for different mass parameter regions are presented in Sec. 3. We also discuss relevant constraints on the parameter space. Further discussion and the conclusions are given in Sec. 4. In addition, we present relevant benchmark points and scan plots showing the possible values of the lightest SUSY mass parameter for which the discrepancy (1) can be explained.

2 The limit $\tan \beta \rightarrow \infty$

2.1 Analytical results and approximations

The MSSM tree-level muon mass is given by

$$m_\mu^{\text{tree}} = y_\mu v_d, \quad (8)$$

the product of the muon Yukawa coupling y_μ and the down-type Higgs vacuum expectation value v_d . Radiative muon mass generation in the MSSM requires the tree-level mass to vanish. There are two generic possibilities: either $y_\mu = 0$ or $v_d = 0$. In case $y_\mu = 0$, the muon mass can be generated from loop diagrams involving binos and smuons and the non-standard soft supersymmetry breaking term A'_μ . The value of a_μ in this scenario has already been studied in Refs. [19,20], and the observed deviation in a_μ can indeed be explained for bino and smuon masses around 1 TeV. A similar study has been performed with the holomorphic trilinear coupling in Ref. [21].

Here we consider the second possibility $v_d = 0$, or equivalently the limit of Eq. (3). In the following we explain the relevant formulas governing the muon mass, Yukawa coupling, and magnetic moment in this limit.

The physical muon (pole) mass m_μ is given by the on-shell muon self energy²

$$m_\mu = -\Sigma_\mu^{\text{MSSM}} \equiv y_\mu v_u \Delta_\mu^{\text{red}}. \quad (9)$$

The explicit result can be found in the Appendix. This equation is used to determine the value of the muon Yukawa coupling y_μ .

²All the following formulas are given for the limit $\tan \beta \rightarrow \infty$. The formulas valid exactly also for arbitrary (small, large or infinite) $\tan \beta$ can easily be reconstructed by replacing $\Delta_\mu^{\text{red}} \rightarrow \frac{v_d}{v_u} + \Delta_\mu^{\text{red}}$, in Eqs. (9, 12, 13).

Eq. (9) also defines the “reduced” self energy factor Δ_μ^{red} (which satisfies $\Delta_\mu = \tan\beta \Delta_\mu^{\text{red}}$ with the usual definition for Δ_μ [23] and which agrees with the quantity ϵ_μ of Ref. [25]). The definition highlights the physics behind the muon mass generation: chiral symmetry (under which left- and right-handed muon transform with different phases) is broken by the Yukawa coupling, and the muon mass is generated by loop-induced couplings of the muon to the vacuum expectation value of the “wrong” Higgs doublet v_u . Hence the factor $y_\mu v_u$ can be pulled out of all contributions to the muon mass. (Another factor of the Higgsino mass μ could also be pulled out of all contributions, because μ has to appear in all couplings of the muon to v_u due to Peccei-Quinn symmetry.) It should be noted that the coupling constants, mixing matrices, and mass eigenvalues entering the self energy partially depend on the muon Yukawa coupling, so Δ_μ^{red} has a small residual dependence on y_μ .

The combination

$$y_\mu v_u \equiv m_\mu \tan\beta^{\text{eff}} \quad (10)$$

is thus an important quantity. In the standard case with moderate $\tan\beta$ it is strictly equal to $m_\mu^{\text{tree}} \tan\beta$ and also often identified with $m_\mu \tan\beta$, but the latter identification is only possible if either higher-order effects can be ignored or on-shell renormalization is used. Here we have to distinguish m_μ from m_μ^{tree} and $\tan\beta^{\text{eff}}$ from $\tan\beta$.

The physics behind the generation of a_μ is the same as for the muon mass. To highlight this similarity we write

$$a_\mu^{\text{SUSY}} = \frac{y_\mu v_u}{m_\mu} a_\mu^{\text{red}}, \quad (11)$$

introducing another dimensionless “reduced” quantity a_μ^{red} . In the standard case, we simply have $a_\mu^{\text{SUSY}} \approx \tan\beta a_\mu^{\text{red}}$. Again, a_μ^{red} has only a small residual dependence on y_μ , and its explicit result can be found in the Appendix.

Combining the equations for the muon mass generation and the magnetic moment, we obtain the MSSM prediction in the limit $\tan\beta \rightarrow \infty$:

$$a_\mu^{\text{SUSY}} = \frac{a_\mu^{\text{red}}}{\Delta_\mu^{\text{red}}}. \quad (12)$$

We record here further useful relations between the quantities introduced so far:

$$a_\mu^{\text{SUSY}} = \tan\beta^{\text{eff}} a_\mu^{\text{red}}, \quad y_\mu = \frac{m_\mu}{v_u \Delta_\mu^{\text{red}}}, \quad \tan\beta^{\text{eff}} = \frac{1}{\Delta_\mu^{\text{red}}} \approx 1650 y_\mu. \quad (13)$$

In contrast to Eqs. (4,6) from the Introduction, the exact result Eq. (12) depends on five independent SUSY mass parameters: the Higgsino mass μ , the gaugino (bino and wino) masses $M_{1,2}$, and the left- and right-handed smuon soft

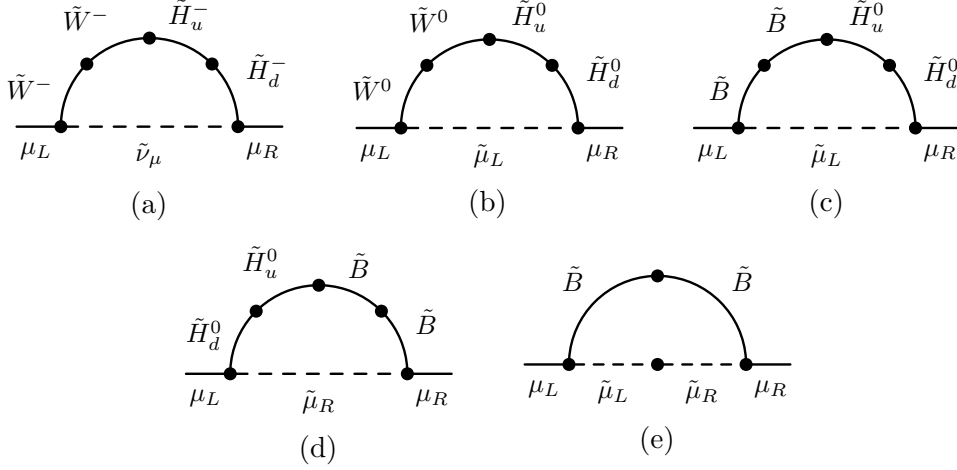


Figure 1: Mass-insertion diagrams contributing to Σ_μ^{MSSM} and a_μ^{SUSY} . For the latter, an external photon couples to any of the charged particles in the loop.

mass parameters $m_{L,R}$. The result has interesting symmetry properties due to cancellations between numerator and denominator: on the one hand, a_μ^{SUSY} is invariant under a change of sign of μ and, on the other, it is invariant under a simultaneous change of signs of M_1 and M_2 . This constitutes a fundamental difference compared to the MSSM with finite $\tan\beta$, where the sign of a_μ^{SUSY} can directly be specified via the sign of μ as e.g. in Eq. (4).

Now, useful approximate formulas for the MSSM muon self energy and the SUSY contribution to the anomalous magnetic moment of the muon are provided. We restrict our considerations to real mass parameters μ , $M_{1,2}$, and taking advantage of the above-mentioned symmetries we choose, without loss of generality, μ and M_1 to be positive. Only the sign of M_2 remains arbitrary. Under the assumption $M_Z \ll M_{\text{SUSY}}$, the SUSY contributions are given by the five mass-insertion diagrams in Fig. 1 [27,28,46]. The self energy factor Δ_μ^{red} can then be decomposed as the sum of

$$\Delta_\mu^{\text{red}}(\tilde{W}\tilde{H}\tilde{\nu}) = -\frac{g_2^2}{16\pi^2} M_2\mu I(M_2, \mu, m_L), \quad (14a)$$

$$\Delta_\mu^{\text{red}}(\tilde{W}\tilde{H}\tilde{\mu}_L) = -\frac{g_2^2}{32\pi^2} M_2\mu I(M_2, \mu, m_L), \quad (14b)$$

$$\Delta_\mu^{\text{red}}(\tilde{B}\tilde{H}\tilde{\mu}_L) = \frac{g_1^2}{32\pi^2} M_1\mu I(M_1, \mu, m_L), \quad (14c)$$

$$\Delta_\mu^{\text{red}}(\tilde{B}\tilde{H}\tilde{\mu}_R) = -\frac{g_1^2}{16\pi^2} M_1\mu I(M_1, \mu, m_R), \quad (14d)$$

$$\Delta_\mu^{\text{red}}(\tilde{B}\tilde{\mu}_L\tilde{\mu}_R) = \frac{g_1^2}{16\pi^2} M_1\mu I(M_1, m_L, m_R), \quad (14e)$$

where $g_{1,2}$ are the U(1) and SU(2) gauge couplings, and the loop function is given

by

$$I(a, b, c) = \frac{a^2 b^2 \ln \frac{a^2}{b^2} + b^2 c^2 \ln \frac{b^2}{c^2} + c^2 a^2 \ln \frac{c^2}{a^2}}{(a^2 - b^2)(b^2 - c^2)(a^2 - c^2)}. \quad (15)$$

This loop function is dimensionful and scales as $1/M^2$, where M denotes the largest of the three mass arguments. The result for the self energy corresponds to the one from Ref. [23] if the limit $\tan \beta \rightarrow \infty$ is taken.

Likewise, for the case $M_Z \ll M_{\text{SUSY}}$, the SUSY contribution to the anomalous magnetic moment of the muon can be approximated by the sum of the expressions

$$a_\mu^{\text{red}}(\tilde{W}\tilde{H}\tilde{\nu}) = -\frac{g_2^2}{8\pi^2} m_\mu^2 \frac{M_2 \mu}{m_L^4} F_a \left(\frac{M_2^2}{m_L^2}, \frac{\mu^2}{m_L^2} \right), \quad (16a)$$

$$a_\mu^{\text{red}}(\tilde{W}\tilde{H}\tilde{\mu}_L) = -\frac{g_2^2}{16\pi^2} m_\mu^2 \frac{M_2 \mu}{m_L^4} F_b \left(\frac{M_2^2}{m_L^2}, \frac{\mu^2}{m_L^2} \right), \quad (16b)$$

$$a_\mu^{\text{red}}(\tilde{B}\tilde{H}\tilde{\mu}_L) = \frac{g_1^2}{16\pi^2} m_\mu^2 \frac{M_1 \mu}{m_L^4} F_b \left(\frac{M_1^2}{m_L^2}, \frac{\mu^2}{m_L^2} \right), \quad (16c)$$

$$a_\mu^{\text{red}}(\tilde{B}\tilde{H}\tilde{\mu}_R) = -\frac{g_1^2}{8\pi^2} m_\mu^2 \frac{M_1 \mu}{m_R^4} F_b \left(\frac{M_1^2}{m_R^2}, \frac{\mu^2}{m_R^2} \right), \quad (16d)$$

$$a_\mu^{\text{red}}(\tilde{B}\tilde{\mu}_L\tilde{\mu}_R) = \frac{g_1^2}{8\pi^2} m_\mu^2 \frac{\mu}{M_1^3} F_b \left(\frac{m_L^2}{M_1^2}, \frac{m_R^2}{M_1^2} \right), \quad (16e)$$

corresponding to the mass-insertion diagrams in Fig. 1, with an external photon coupling to the charged internal line. Via Eq. (11), this result can be related to the one for finite $\tan \beta$ quoted e.g. in Refs. [28, 33], where the loop functions

$$F_a(x, y) = -\frac{F_2^C(x) - F_2^C(y)}{3(x - y)}, \quad (17a)$$

$$F_b(x, y) = -\frac{F_2^N(x) - F_2^N(y)}{6(x - y)} \quad (17b)$$

have been introduced. The functions F_2^C and F_2^N can be found in the Appendix.

We now provide seminumerical approximations which allow to directly read off numerical orders of magnitude and signs and which facilitate the phenomenological discussion. The dimensionless loop functions

$$\hat{I} \left(\frac{a}{c}, \frac{b}{c} \right) = ab I(a, b, c), \quad (18a)$$

$$\hat{K}_N(x, y) = 2xy F_b(x, y), \quad (18b)$$

$$\hat{K}_W(x, y) = 2xy [2F_a(x, y) - F_b(x, y)], \quad (18c)$$

are especially useful if the sign and size of the different contributions shall be compared. The first two of these functions have been introduced in Refs. [24] and

[29] respectively. In the special case of three equal masses, we get $\hat{I}(1, 1) = 1/2$, $\hat{K}_W(1, 1) = 5/6$ and $\hat{K}_N(1, 1) = 1/6$. In general, \hat{I} and \hat{K}_N lie between 0 and 1; \hat{K}_W lies between 0 and 1.155. Furthermore, in the case of equal arguments, $\hat{I}(x, x)$ and $\hat{K}_N(x, x)$ increase monotonically, while $\hat{K}_W(x, x)$ increases up to a value of about 1.155 at $x \approx 11.15$ and then decreases towards a limit of 1 for $x \rightarrow \infty$.

By inserting all numerically known Standard Model quantities, the negative MSSM muon self energy, which should be equal to the muon mass [see Eq. (9)], can be written as

$$\begin{aligned}
m_\mu &= y_\mu v_u \Delta_\mu^{\text{red}} \\
&\approx y_\mu \left[-\text{sign}(M_2) 0.705 \text{ GeV } \hat{I} \left(\frac{|M_2|}{m_L}, \frac{\mu}{m_L} \right) \right. \\
&\quad + 0.067 \text{ GeV } \hat{I} \left(\frac{M_1}{m_L}, \frac{\mu}{m_L} \right) \\
&\quad - 0.135 \text{ GeV } \hat{I} \left(\frac{M_1}{m_R}, \frac{\mu}{m_R} \right) \\
&\quad \left. + 0.135 \text{ GeV } \hat{I} \left(\frac{M_1}{m_R}, \frac{m_L}{m_R} \right) \frac{\mu}{m_L} \right],
\end{aligned} \tag{19}$$

where the order of terms is the same as in Eqs. (14), and the first term combines the contributions from loops with charged or neutral winos.

Similarly, we derive the numerical approximation for a_μ^{SUSY} as

$$\begin{aligned}
a_\mu^{\text{SUSY}} &= \frac{y_\mu v_u}{m_\mu} a_\mu^{\text{red}} \\
&\approx y_\mu \left[\text{sign}(M_2) 2.483 \times 10^{-8} \frac{(1 \text{ TeV})^2}{\mu |M_2|} \hat{K}_W \left(\frac{M_2^2}{m_L^2}, \frac{\mu^2}{m_L^2} \right) \right. \\
&\quad + 0.712 \times 10^{-8} \frac{(1 \text{ TeV})^2}{\mu M_1} \hat{K}_N \left(\frac{M_1^2}{m_L^2}, \frac{\mu^2}{m_L^2} \right) \\
&\quad - 1.425 \times 10^{-8} \frac{(1 \text{ TeV})^2}{\mu M_1} \hat{K}_N \left(\frac{M_1^2}{m_R^2}, \frac{\mu^2}{m_R^2} \right) \\
&\quad \left. + 1.425 \times 10^{-8} \frac{\mu M_1 (1 \text{ TeV})^2}{m_L^2 m_R^2} \hat{K}_N \left(\frac{m_L^2}{M_1^2}, \frac{m_R^2}{M_1^2} \right) \right],
\end{aligned} \tag{20}$$

which corresponds to the result from Ref. [29] in the limit $\tan \beta \rightarrow \infty$ and combines the contributions that are created by a charged or neutral internal wino in the first term.

The approximate expressions (19) and (20) have several noteworthy features.

- They are linear in y_μ because the residual dependence of Δ_μ^{red} and a_μ^{red} on y_μ vanishes for $M_Z/M_{\text{SUSY}} \rightarrow 0$.

- All terms involve the factor μM_1 or μM_2 . This explains the symmetry of a_μ^{SUSY} (given by Eq. (12)) under a sign change either of μ or of M_1 and M_2 .
- Under sign change of M_2 alone, the wino contributions change their signs relative to the bino contributions.
- The signs of the contributions are related: each mass-insertion diagram contributes with equal sign to Δ_μ^{red} and a_μ^{red} , except for the chargino diagram, where the signs are opposite.
- Thus if the chargino diagram (a) in Fig. 1 dominates in both Δ_μ^{red} and a_μ^{red} , we get $a_\mu^{\text{SUSY}} < 0$. In contrast, for neutralino dominance a_μ^{SUSY} becomes positive and, therefore, has the correct sign with regard to an explanation of the discrepancy (1).
- The contributions (14b) and (16b) from the diagram with an internal neutral wino can never dominate since they are always smaller than the ones from the diagram with an internal charged wino. In Δ_μ^{red} , the charged and neutral wino contribution add constructively, in a_μ^{red} destructively.

2.2 Experimental constraints from other sectors

Before we present our numerical analyses, we briefly discuss constraints on parameter space from other observables and sectors and show that the arising constraints can be satisfied without restricting the five parameters $\mu, M_{1,2}, m_{L,R}$ relevant for a_μ . Clearly, an observable strongly related to a_μ is the lepton flavour violating decay $\mu \rightarrow e\gamma$. The correlation of the two MSSM predictions has been discussed extensively in the literature [49, 57–60]. If the prediction for a_μ^{SUSY} is fixed, the SUSY prediction for $\mu \rightarrow e\gamma$ can be estimated quite well up to the unknown lepton flavour violating parameters. In particular the one-loop amplitudes for the two quantities share the same $\tan\beta$ enhancement; the correlation between the two does not strongly depend on $\tan\beta$. E.g. Figs. 13–16 of Ref. [49] remain valid also for $\tan\beta \rightarrow \infty$. Therefore, like for moderate $\tan\beta$, the decay $\mu \rightarrow e\gamma$ is compatible with experimental bounds [61] for sufficiently small lepton flavour violating parameters.

Further constraints from B -physics have been discussed extensively in Ref. [25]; taking the limits of those results as $\tan\beta \rightarrow \infty$ shows that agreement between theory and experiment can be achieved. The parameters mainly constrained by B -physics are the heavy Higgs boson masses as well as the stop trilinear coupling A_t . Since these parameters are not relevant for the discussion of a_μ , we give only a brief account of how they are constrained. The new physics contribution to $\text{BR}(B^+ \rightarrow \tau^+\nu)$ can be suppressed below 2σ with σ being the experimental error, by having the charged Higgs mass M_{H^\pm} around a few TeV or higher. We can relax the constraints from $B_s \rightarrow \mu^+\mu^-$ and $B \rightarrow X_s\gamma$ by

assuming that A_t and flavour-violating squark mass insertions are small enough. In addition, the former process can be further suppressed by raising the masses of the CP -odd as well as the CP -even heavier Higgses, and the latter by increasing the squark masses.

Given large bottom and tau Yukawa couplings, large sbottom and stau corrections to the mass of the lighter CP -even Higgs h might undermine the stop contribution that should lift m_h up to the measured value around 125 GeV [62], as $\tan\beta \rightarrow \infty$. Indeed, Fig. 2 of Ref. [63] shows a rapid drop of m_h as $\tan\beta$ grows over around 40. This happens due to a cancellation between the tree-level and the Δ_b contributions to the bottom quark pole mass causing a blow-up of the bottom Yukawa coupling. As mentioned in the same reference, this is however not necessarily the case for a high $\tan\beta$. First of all, it never happens for $\mu < 0$. Even if $\mu > 0$, once we enter the regime where $|\Delta_b| \gg 1$, the bottom Yukawa coupling comes back to $\mathcal{O}(1)$, thereby suppressing its negative contribution to m_h . Therefore the $\tan\beta \rightarrow \infty$ scenario allows to choose third generation sfermion masses which lead to a correct Higgs mass.

Owing to decoupling of the multi-TeV extra Higgs masses required by the B -physics constraints, the MSSM Higgs sector is approximately SM-like [64]. Nonetheless it is instructive to discuss the most relevant SM-like Higgs decay modes, $h \rightarrow b\bar{b}$, $h \rightarrow \tau^+\tau^-$, and $h \rightarrow \mu^+\mu^-$, which might potentially be affected by large bottom and charged lepton Yukawa couplings. Their decay rates can be kept close to the SM values in the following way. The effective H_u^0 - f - f coupling, for $f = b, \tau, \mu$, is generated by the same loop diagrams that generate m_f . Therefore, the h - f - f coupling should be SM-like if h consists purely of H_u^0 to a sufficient extent. Remember that the H_d^0 - f - f coupling, y_f , can be comparable to or even larger than y_t . The remaining question is then how to maintain the Higgs mixing angle α small enough for h to avoid excessive H_d^0 -contamination. It is easy to see that the 2×2 tree-level CP -even Higgs mass matrix becomes diagonal as $\tan\beta \rightarrow \infty$ (see e.g. Eq. (23) of Ref. [65]). We can then suppress the one-loop corrections to its off-diagonal elements by setting A_t and A_b to zero, as is apparent e.g. from Eq. (26) of Ref. [65] and Eq. (3) of Ref. [63]. Regarding $h \rightarrow \gamma\gamma$, we can use the fact that the stau-loop contribution (see e.g. Refs. [52–54]) to the dimension-five effective operator decouples faster than the tau self energy, as the stau masses increase.

3 Numerical analysis

3.1 Dominance transition and sign change

In the Introduction we have shown that if all SUSY masses are equal, a_μ^{SUSY} becomes negative in the limit of $\tan\beta \rightarrow \infty$. In this case the wino contributions dominate in both a_μ^{red} and Δ_μ^{red} , i.e. in the numerator and denominator of Eq. (12),

and they have opposite signs, see Eqs. (19,20). However, these equations also show that the resulting a_μ^{SUSY} will be positive if any of the three bino contributions dominates.

In the following we will delineate regions in the five-dimensional parameter space of the masses $M_{1,2}$, μ , $m_{L,R}$ in which a_μ^{SUSY} is positive. We start by noting that the signs only depend on mass ratios and that each of the three bino contributions can be expected to dominate if a particular mass hierarchy is valid:

- The $\tilde{B}\tilde{\mu}_L\tilde{\mu}_R$ contributions dominate for $M_1, m_L, m_R \ll \mu$: “large μ -limit”
- The $\tilde{B}\tilde{H}\tilde{\mu}_R$ contributions dominate for $M_1, \mu, m_R \ll m_L$: “ $\tilde{\mu}_R$ -dominance”
- The $\tilde{B}\tilde{H}\tilde{\mu}_L$ contributions dominate for $M_1, \mu, m_L \ll |M_2|, m_R$. These have the smallest numerical prefactors, and we can expect them to dominate only for rather extreme hierarchies.³

The phenomenological behaviour and importance of the $\tilde{B}\tilde{\mu}_L\tilde{\mu}_R$ and $\tilde{B}\tilde{H}\tilde{\mu}_R$ contributions have also been discussed recently in various contexts in Refs. [29–33, 40, 49] and Refs. [32, 33, 48, 49], respectively. We first focus on cases where these two contributions become dominant. Parameter regions in which the $\tilde{B}\tilde{H}\tilde{\mu}_L$ contributions dominate will be presented later on.

Fig. 2 illustrates plots of the individual contributions to a_μ^{red} and Δ_μ^{red} for parameters which interpolate between the equal SUSY mass case and the two mass hierarchies for either “large μ -limit”, Fig. 2(a), or “ $\tilde{\mu}_R$ -dominance”, Fig. 2(b). In each hierarchy case the desired bino contributions become the largest ones for sufficiently large mass ratios. We first discuss Fig. 2(a), corresponding to the “large μ -limit”, in detail. It shows the contributions as functions of the ratio $|M_2| = \mu$ over $M_1 = m_L = m_R$; the horizontal axis is given by $x = \log_{10}(\mu/m_R)$. We pay particular attention to the dominance transition among the contributions and the sign change of a_μ^{red} and Δ_μ^{red} .

- Around $x = 0$, where all masses are equal, the wino contribution dominates in both a_μ^{red} and Δ_μ^{red} . For larger values of x , the $\tilde{B}\tilde{\mu}_L\tilde{\mu}_R$ contributions increase proportionally to μ whereas the other contributions are suppressed as $1/\mu$. Hence the latter tend to zero for large x , except for the $\tilde{W}\tilde{H}\tilde{L}$ contribution to Δ_μ^{red} , which tends to a constant because it is also proportional to M_2 and $|M_2| = \mu$ in this plot.
- At $x \approx 0.36$, the dominant contribution to a_μ^{red} changes from the wino contribution to the $\tilde{B}\tilde{\mu}_L\tilde{\mu}_R$ contribution. For larger mass ratios, $x \approx 1.00$, the same dominance change also happens in Δ_μ^{red} and thus a_μ^{SUSY} is always positive for $x > 1$.

³Dominance of the $\tilde{B}\tilde{H}\tilde{\mu}_L$ contributions can also be achieved with $|M_2| \ll M_1, \mu, m_L \ll m_R$. We will not investigate this below since the mass hierarchies would be even more extreme.

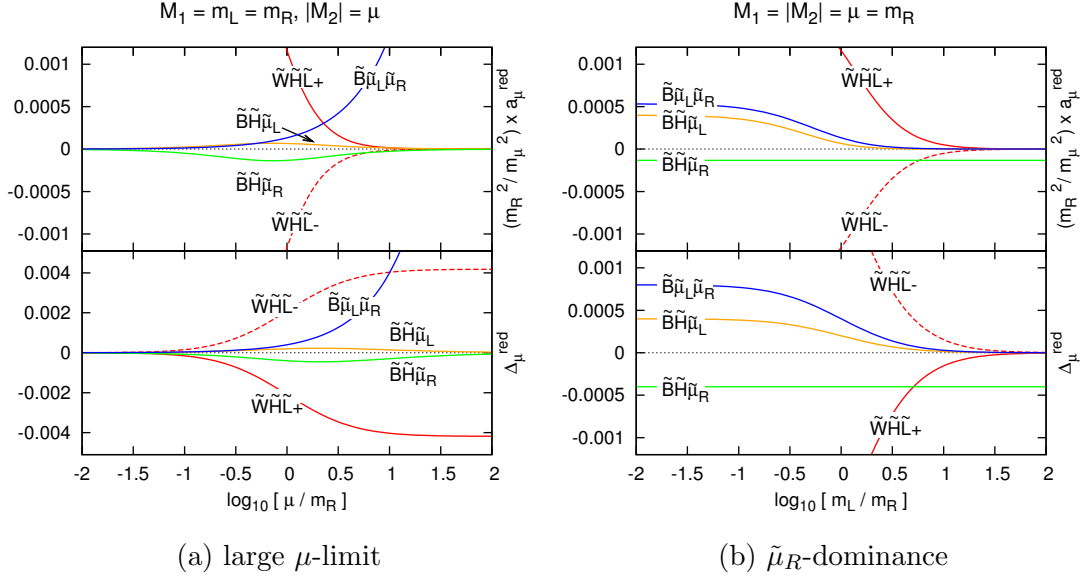


Figure 2: Individual behaviour of the contributions to a_μ^{red} and Δ_μ^{red} for two different mass spectra. The full result a_μ^{SUSY} is given by Eq. (12) as the ratio of the sums of the contributions. $\tilde{W}\tilde{H}\tilde{L}\pm$ denotes the sum of $\tilde{W}\tilde{H}\tilde{\nu}$ and $\tilde{W}\tilde{H}\tilde{\mu}_L$, for positive or negative M_2 , respectively. In the upper plots, the individual contributions to a_μ^{red} are rescaled by m_R^2/m_μ^2 to make the results depend only on ratios of SUSY masses.

- In the intermediate region, $0.36 < x < 1.00$, $\tilde{B}\tilde{\mu}_L\tilde{\mu}_R$ already dominates in the numerator but the wino contribution still dominates in the denominator of a_μ^{SUSY} . Here the sign of a_μ^{SUSY} depends on M_2 in such a way that it is equal to $\text{sign}(-M_2)$.
- For $x < 0$, the wino contributions remain dominant.

Similarly, we discuss Fig. 2(b), which corresponds to “ $\tilde{\mu}_R$ -dominance”. It shows the contributions as functions of the ratio m_L over $M_1 = |M_2| = \mu = m_R$; the horizontal axis is given by $x = \log_{10}(m_L/m_R)$.

- Like in Fig. 2(a), the equal mass case emerges at $x = 0$, and around this point the wino contributions dominate in both the numerator and denominator of a_μ^{SUSY} . For larger x , all contributions tend to zero except for the $\tilde{B}\tilde{H}\tilde{\mu}_R$ ones, which are independent of m_L and thus stay constant.
- At $x \approx 0.7$, the $\tilde{B}\tilde{H}\tilde{\mu}_R$ contributions become dominant; accidentally, the dominance change occurs approximately at the same x in the numerator and denominator. For larger values of x , this leads to a positive a_μ^{SUSY} , independently of the sign of M_2 .

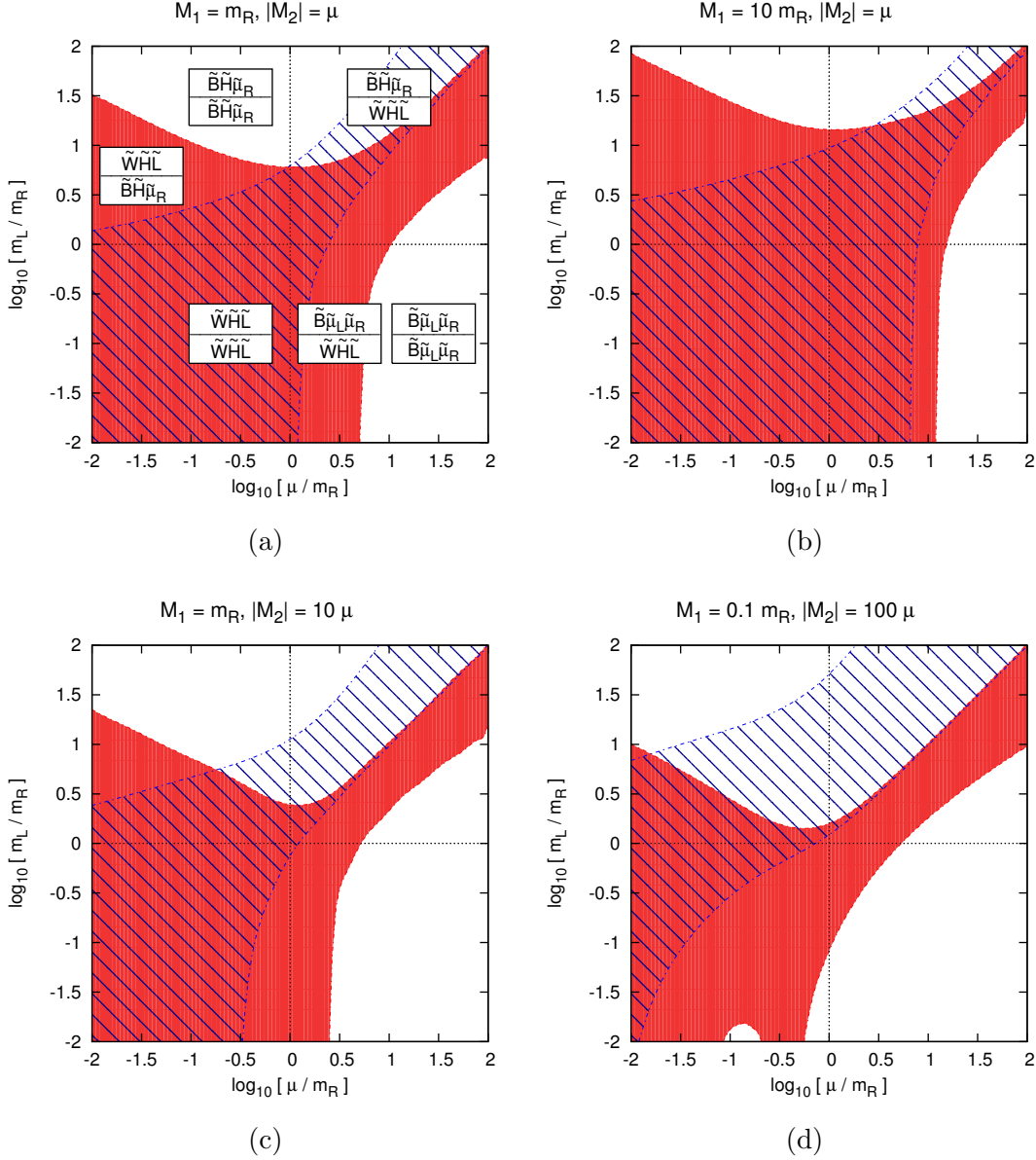


Figure 3: Signs of a_μ^{SUSY} in the plane of m_L/m_R versus μ/m_R , for the two possible signs of M_2 . In the white regions a_μ^{SUSY} is positive. The red regions indicate negative a_μ^{SUSY} for $M_2 > 0$, the blue hatched ones negative a_μ^{SUSY} for $M_2 < 0$. In the overlap regions a_μ^{SUSY} is always negative. The first plot also displays which contributions dominate in the bulk of each region in the numerator and denominator of Eq. (12). (It should be noted that near the borders between the regions there are cancellations, and different contributions can be the largest.) In each plot the remaining two mass ratios M_1/m_R and $|M_2|/\mu$ are fixed as indicated; the structure of the dominance regions is the same in all plots. For the small white region in the bottom left area of plot (d), see the text.

To investigate the sign of a_μ^{SUSY} comprehensively we plot it in a more general parameter space, as a function of the two mass ratios used in Figs. 2(b) and (a), i.e. in the plane m_L/m_R versus μ/m_R . Fig. 3 displays the results for four different choices of the remaining mass ratios M_1/m_R and $|M_2|/\mu$. We begin by discussing Fig. 3(a). It generalizes Fig. 2 by assuming $M_1 = m_R$ and $|M_2| = \mu$, so the different regions in Fig. 3(a) can be fully understood from the previous discussion.

- The large, central red/blue overlap region contains the origin at which all relevant SUSY masses are equal. In this region the wino contributions dominate and a_μ^{SUSY} is always negative.
- The two white regions, where a_μ^{SUSY} is always positive, correspond to the “large μ -limit” and the “ $\tilde{\mu}_R$ -dominance” region.
- The blue hatched and the red regions (excluding the red/blue overlap) are transition regions where different contributions dominate in numerator and denominator. They generalize the region $0.36 < x < 1.00$ of Fig. 2(a). Here the sign of a_μ^{SUSY} depends on M_2 and is equal to the sign of either $(+M_2)$ (blue hatched) or $(-M_2)$ (red).

In Fig. 3(a), the gaugino masses $|M_2|$ and M_1 are equated with μ and m_R , respectively. This is a reasonable choice since their precise values are qualitatively unimportant for the appearance of the different regions. The dependence on these two gaugino masses is investigated in Figs. 3(b)–(d), whose presentation is similar to Fig. 3(a) but with either $M_1 = 10 m_R$, $|M_2| = 10 \mu$, or $M_1 = 0.1 m_R$ and $|M_2| = 100 \mu$. Together, these plots cover large, representative parts of the full parameter space of the four relevant mass ratios.

Obviously, all plots can be understood in the same way as Fig. 3(a). As M_1 becomes heavier than m_R in Fig. 3(b), the bino contributions are suppressed, the wino-dominance area expands, and the positive a_μ^{SUSY} regions shrink. In contrast, the positive a_μ^{SUSY} regions expand in Figs. 3(c) and (d), since M_2 gets heavier than μ and the wino contributions are thereby suppressed.

Finally we investigate the positive a_μ^{SUSY} region with $\tilde{B}\tilde{H}\tilde{\mu}_L$ dominance, which cannot be seen for the most part in the previous graphs. This dominance can be realized under the hierarchy condition $M_1, \mu, m_L \ll |M_2|, m_R$, which is satisfied in the small white region in the bottom left area of Fig. 3(d). To better understand the $\tilde{B}\tilde{H}\tilde{\mu}_L$ dominance, we change the plot axes to the ones of Fig. 4(a). Here the sign of a_μ^{SUSY} as well as information about which contributions dominate in a_μ^{red} and Δ_μ^{red} are displayed in the plane of m_R/μ versus M_1/μ . Fig. 4(b) corresponds to the y -axis of Fig. 4(a) and shows the individual behaviour of each contribution. As we can see, the $\tilde{B}\tilde{H}\tilde{\mu}_L$ contributions dominate only for extreme mass ratios $m_R/\mu \gtrsim 100$.

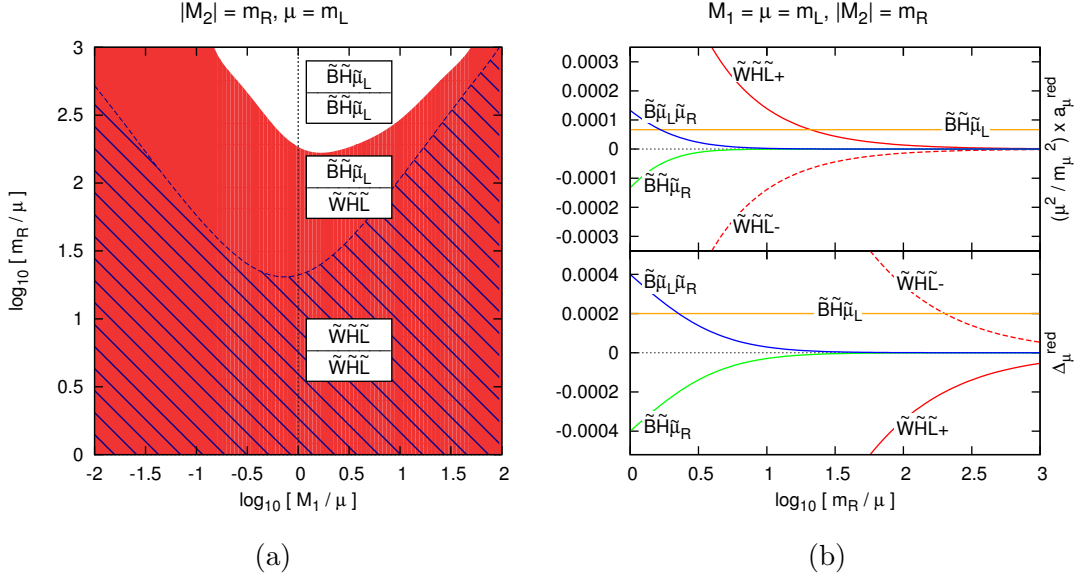


Figure 4: (a) Signs of a_μ^{SUSY} in the plane of m_R/μ versus M_1/μ , for the two possible signs of M_2 . The colour coding is the same as in Fig. 3. (b) Individual behaviour of the contributions to a_μ^{red} and Δ_μ^{red} as a function of the mass ratio m_R/μ . The presentation is analogous to Fig. 2.

3.2 Magnitude of a_μ^{SUSY} and constraints on Yukawa couplings

Having understood the parameter regions which lead to positive a_μ^{SUSY} , we now turn our interest to its magnitude and also take into account other constraints on the parameter space. As discussed in the Introduction, we can write

$$a_\mu^{\text{SUSY}} = C \frac{m_\mu^2}{M_{\text{SUSY},\text{min}}^2}, \quad C = \mathcal{O}(1), \quad (21)$$

where $M_{\text{SUSY},\text{min}}$ is the smallest among the five relevant mass parameters M_1 , $|M_2|$, μ , and $m_{L,R}$ [and thus similar but not equal to the lightest SUSY particle (LSP) mass since the latter arises from diagonalization of mass matrices]. The coefficient C is expected to be of order unity because of radiative muon mass generation. It depends only on the four independent mass ratios (up to terms suppressed by powers of M_Z^2/M_{SUSY}^2). Hence for each given set of mass ratios we can pose two questions:

1. What is the value of C ?
2. What is the minimum SUSY mass for which $a_\mu^{\text{SUSY}} = 28.7 \times 10^{-10}$?

The answers are given in Fig. 5 for the special choices $M_1 = m_R$ and $|M_2| = \mu$ which have already been used in Fig. 3(a). The figures also show the behaviour

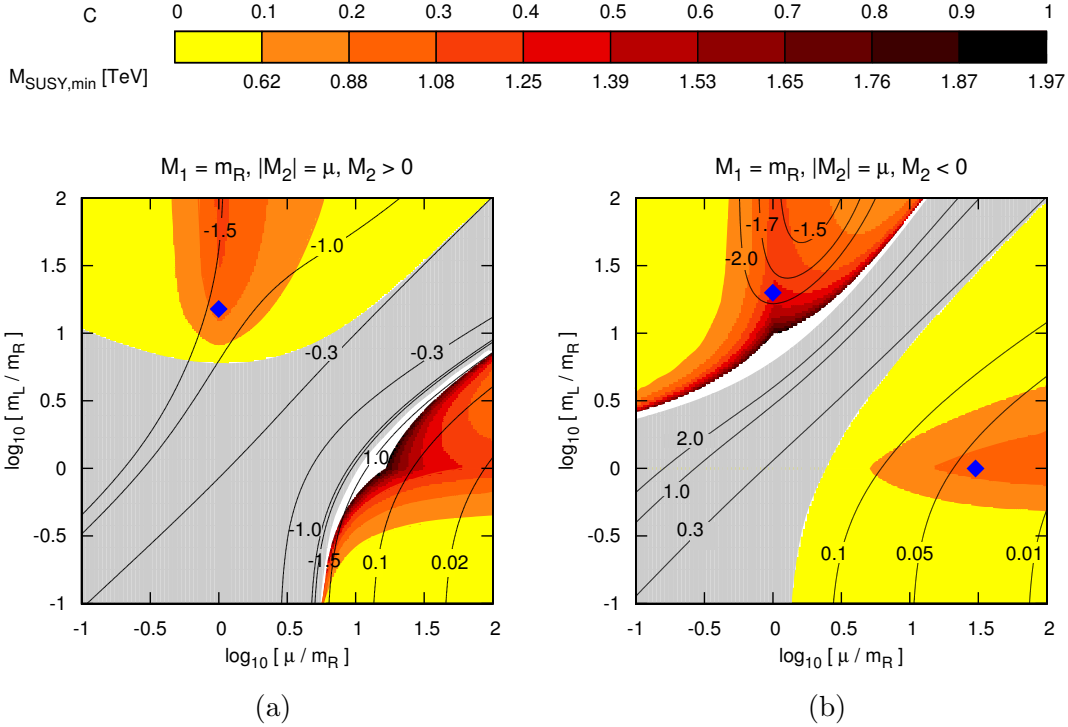


Figure 5: Magnitude of a_μ^{SUSY} and muon Yukawa coupling y_μ in the plane of m_L/m_R versus μ/m_R , for positive M_2 (left) and negative M_2 (right). The colour coding corresponds to the different values of the coefficient C defined in Eq. (21) and the equivalent minimum SUSY mass which leads to agreement with the current deviation via $a_\mu^{\text{SUSY}} = 28.7 \times 10^{-10}$. The black contours correspond to the indicated values of the muon Yukawa coupling resulting from Eq. (9). The grey regions are excluded by negative a_μ^{SUSY} . In the white regions the denominator Δ_μ^{red} undergoes a sign change, and the perturbation theory becomes untrustworthy due to large y_μ . Benchmark parameter points introduced in Table 1 are marked with blue squares.

of the muon Yukawa coupling, which is proportional to $1/\Delta_\mu^{\text{red}}$, see Eq. (13). The four most interesting regions are the “large μ -limit” and “ $\tilde{\mu}_R$ -dominance” regions with either positive or negative M_2 . These are located in the right end and middle top areas of the two plots and correspond to the white regions of Fig. 3(a) with a positive a_μ^{SUSY} . In detail Fig. 5 shows the following.

- The first important observation is that in the centre of the “large μ -limit” and “ $\tilde{\mu}_R$ -dominance” regions, C lies between 0.2 and 0.4; the corresponding minimum SUSY mass is around 1 TeV. C does not quite reach unity because of the behaviour of the loop functions in Δ_μ^{red} and a_μ^{red} .
- In both regions, the magnitude of C , the minimum SUSY mass, and the

muon Yukawa coupling depend on the sign of M_2 . This dependence arises from interference of the dominant contributions with subdominant wino contributions, which can be either constructive in Δ_μ^{red} and destructive in a_μ^{red} or vice versa.

- There are small white strips in parameter space with larger C and minimum SUSY masses. In these strips Δ_μ^{red} undergoes a sign change and the Yukawa coupling becomes infinite. Here perturbation theory is not trustworthy since two-loop effects are non-negligible due to the accidental cancellation of the one-loop contributions. We exclude these regions from further discussion.
- Of particular interest are the regions with smaller Yukawa couplings, i.e. the “large μ -limit” region for negative M_2 and the “ $\tilde{\mu}_R$ -dominance” region for positive M_2 . Here C can still increase up to 0.3, and the minimum SUSY mass reaches up to 1.1 TeV. The opposite sign choices lead to the strips where y_μ diverges. In the “large μ -limit” the muon Yukawa coupling is always proportional to $1/\mu$ and therefore its magnitude is comparatively small and decreasing as μ increases. In the regions of “ $\tilde{\mu}_R$ -dominance” $|y_\mu|$ is generally much larger. Eq. (19) allows to deduce that for “ $\tilde{\mu}_R$ -dominance”, $|y_\mu|$ cannot become smaller than 0.78 for negative M_2 and 0.12 for positive M_2 , respectively.

Now, we consider constraints on the relevant parameter space for large a_μ^{SUSY} . All previous plots are based on the mass-insertion approximation and depend only on mass ratios. For each given set of mass ratios with positive a_μ^{SUSY} there is a value of the overall mass scale M_{SUSY} for which a_μ^{SUSY} agrees with experiment. In the following discussions we always fix M_{SUSY} to that particular scale.

Fig. 6 shows the same parameter space as Fig. 5, but displays regions in which charged SUSY masses become too small (medium grey), the muon Yukawa coupling is non-perturbative (dark grey) or the electroweak vacuum becomes unstable (hatched). In detail, the constraints are the following:

- The light grey regions, which have already been shown in Fig. 5, yield negative values of a_μ^{SUSY} and are thus not of interest with regard to an explanation of the discrepancy (1).
- There are strong but model-dependent collider bounds on the masses of charged SUSY particles. Here we are interested in very large electroweak SUSY masses, which are far above the LHC limits. Therefore we show as the medium grey regions in Fig. 6 an exemplary contour corresponding to a chargino or smuon which is lighter than 100 GeV.
- In the dark grey regions the muon Yukawa coupling violates perturbativity, $|y_\mu| > \sqrt{4\pi}$. Generally, we regard the model as a pure low-energy model and do not require the stronger constraint that there be no Landau poles at

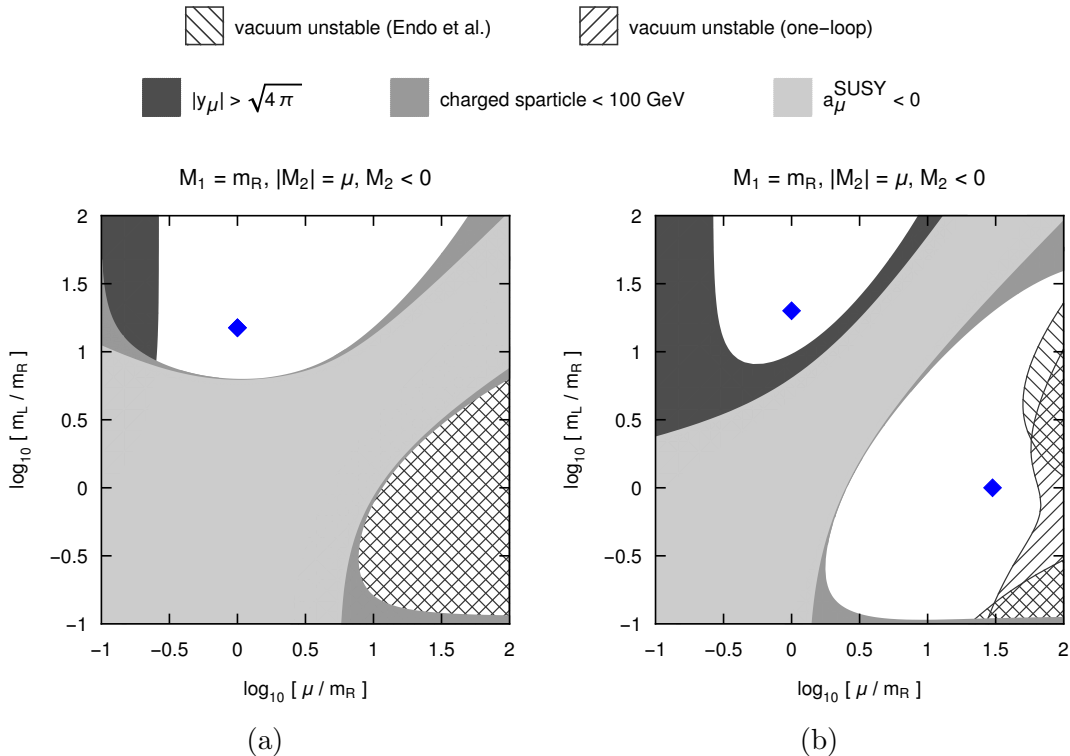


Figure 6: Excluded parameter regions in the plane of m_L/m_R versus μ/m_R , for positive M_2 (left) and negative M_2 (right). The areas corresponding to the different constraints are plotted in the same order as they appear in the legend. Detailed explanations for each constraint can be found in the text. Benchmark parameter points introduced in Table 1 are marked with blue squares.

higher scales; such an analysis has been done in Refs. [24, 25]. It should be further noted that the observable couplings of the lightest Higgs boson are SM-like up to corrections suppressed by powers of the SUSY scale. This is true independently of the value of the fundamental Yukawa coupling due to decoupling.

- As discussed in Refs. [30, 51–54], the combination $y_\ell \mu$ is limited by the requirement that the electroweak vacuum is metastable with a lifetime longer than the age of the universe. This constrains in particular the parameter regions with large μ as already stressed in Ref. [30]. The regions which are excluded by the fitting formula from this reference applied to the muon sector are shown in Fig. 6. Since it is possible that $y_\ell \gtrsim y_t$ in our scenario, the $\mathcal{O}(y_\ell^n)$ counterpart of the standard $\mathcal{O}(y_t^n)$ correction to the effective potential might be significant. To scrutinize the effect of the former, we add to the effective potential the one-loop contributions (see e.g. Eq. (1.2) of Ref. [55]) in the gaugeless limit, with the renormalization scale $Q = \sqrt{m_L m_R}$. They

include the (s)lepton- and the Higgs(ino)- as well as the (s)top-loop contributions. We then evaluate the Euclidean action numerically using the method presented in Ref. [56]. In principle, the metastability bound on $y_{\ell\mu}$ depends on the pseudo-scalar Higgs mass M_A affecting the one-loop correction to the slepton squared mass. Motivated by the B -physics constraints, we set $M_A = 50$ TeV, a high enough value for extra Higgs states to decouple. By applying the specified procedure to the muon sector, we find that the regions shown in Fig. 6 are excluded because of an unstable electroweak vacuum.

According to the results shown in Fig. 6, the requirement of vacuum metastability poses strong constraints on parameter space, in particular on the “large μ -limit” region. This region is completely excluded for positive M_2 , while for negative M_2 the ratio μ/m_R must not be too large. The “ $\tilde{\mu}_R$ -dominance” region is not constrained by vacuum metastability. The two different approaches to the vacuum metastability yield similar results but the influence of the additional terms is visible in Fig. 6(b).

The Yukawa coupling of the τ lepton, which is another quantity of interest, can be determined similarly to y_μ . There is a strong correlation if the stau masses are assumed to be equal to the smuon masses; without this assumption the two Yukawa couplings are basically independent, and vacuum metastability from the tau sector does not further constrain the five-dimensional parameter space. However, a detailed analysis should take into account higher orders in the large tau Yukawa coupling and is beyond the scope of this paper.

Thus we find that out of the four interesting regions in Fig. 5, three survive. Now we briefly comment on the comparison between the approximate results for y_μ as well as a_μ^{SUSY} obtained from Eqs. (14, 16) and their exact results according to the Appendix. In the three viable regions described above, the deviation amounts to at most a few percent. Outside these regions the approximation becomes worse for very small SUSY masses and in the small strips with divergent muon Yukawa coupling.

4 Conclusions

We have studied the muon magnetic moment in the MSSM for $\tan\beta \rightarrow \infty$. This is a viable limit in which all down-type masses are generated by loop-induced couplings to the “wrong” Higgs H_u . The scenario can also be viewed independently of supersymmetry, as a simplified model which realizes the general idea of radiative muon mass generation.

The SUSY contribution to the muon anomalous magnetic moment is given by Eq. (12) as the ratio of two one-loop quantities. For this reason the scenario leads to large a_μ with TeV-scale new physics masses, and it behaves qualitatively very differently from the standard MSSM with $\tan\beta \lesssim 50$. E.g. the signs of gaugino

μ	M_1	M_2	m_L	m_R	$a_\mu^{\text{SUSY}}/10^{-9}$	y_μ	Figure	Characteristic
30	1	-30	1	1	2.80	0.04	5b	large μ -limit
15	1	-1	1	1	3.01	0.09	-	large μ -limit
1	1	1	15	1	2.64	-1.37	5a	$\tilde{\mu}_R$ -dominance
1	1	30	30	1	2.77	-1.18	-	$\tilde{\mu}_R$ -dominance
1.3	1.3	-1.3	26	1.3	2.90	-1.89	5b	$\tilde{\mu}_R$ -dominance

Table 1: Benchmark parameter points. All masses are given in TeV.

and Higgsino masses drop out between numerator and denominator and cannot be used to adjust the overall sign of a_μ^{SUSY} . For equal masses, a_μ^{SUSY} is strictly negative, see Eq. (7). In general, the sign of a_μ^{SUSY} depends on the ratios between the five relevant mass parameters; Figs. 2–4 give a comprehensive explanation of which mass ratios lead to positive a_μ^{SUSY} .

The three most promising parameter regions with positive a_μ^{SUSY} are the “large μ -limit” for negative M_2 and the “ $\tilde{\mu}_R$ -dominance” region for positive or negative M_2 . The “large μ -limit” region with positive M_2 is excluded because of vacuum instability. In all three viable cases, large contributions to a_μ^{SUSY} are possible without conflicts with other experimental constraints, see Figs. 5, 6. The discrepancy (1) can be fully explained with a lightest SUSY mass above 1 TeV.

To conclude, we summarize the behaviour in three simple ways. Table 1 lists several benchmark parameter points with SUSY mass parameters at 1 TeV or higher and gives the resulting a_μ^{SUSY} and muon Yukawa coupling. Two points correspond to the “large μ -limit” with negative M_2 and three to the “ $\tilde{\mu}_R$ -dominance” region with positive or negative M_2 . Some points involve only one heavy and four lighter SUSY masses; for these large a_μ^{SUSY} is possible for less extreme mass splitting than for the ones with two heavy and three lighter masses. The benchmark points further illustrate that the Yukawa coupling is much larger in the case of “ $\tilde{\mu}_R$ -dominance”.

Fig. 7 shows the results of two scans of the five-dimensional parameter space: plotted are the largest possible values of the minimum SUSY mass $M_{\text{SUSY},\text{min}}$ which lead to agreement with Eq. (1). The left panel shows the results as a function of $\log_{10}(m_L/M_1)$ (for positive M_2), it corresponds to the y -axis of Fig. 5(a); the right panel as a function of $\log_{10}(\mu/M_1)$ (for negative M_2), it corresponds to the x -axis of Fig. 5(b). The results correspond to the regions presented in Fig. 5 and are just slightly higher than the values obtained there with fixed mass ratios.

Finally, for the regions of interest, a simple approximation in the style of Eq. (7) can be derived: for the “large μ -limit” region, we consider the limit $|\mu| \gg |M_1| = m_L = m_R \equiv M_{\text{SUSY}}$, and for the “ $\tilde{\mu}_R$ -dominance” region we consider the limit $m_L \gg |\mu| = |M_1| = m_R \equiv M_{\text{SUSY}}$. In both of these limits, we

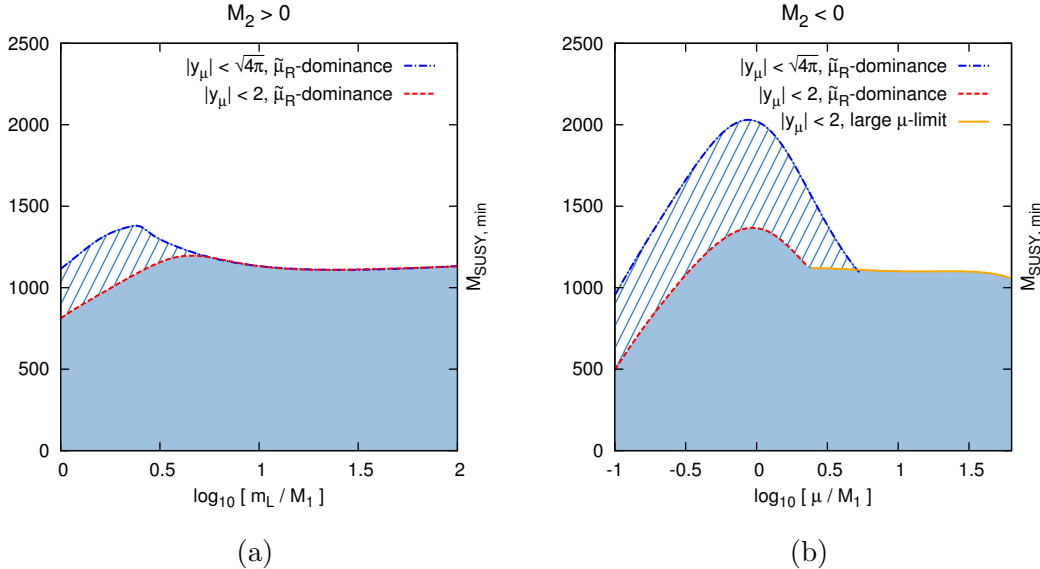


Figure 7: Results of scans over all five relevant SUSY mass parameters. The plots show the maximum values of $M_{\text{SUSY},\text{min}}$ for which the deviation (1) can be explained, also indicating the characteristic of the parameter point for which the maximum is achieved. In some regions the achievable maximum depends on the cutoff on the magnitude of the muon Yukawa coupling, as indicated; in the other regions the maximum is achieved for smaller Yukawa couplings. The scans take into account the constraint of vacuum metastability (one-loop), as discussed in Sec. 3.2, and in the right plot all investigated parameter points with $\log_{10}(\mu/M_1) > 1.8$ are excluded by this.

obtain

$$a_\mu^{\text{SUSY}} \approx 37 \times 10^{-10} \left(\frac{1 \text{ TeV}}{M_{\text{SUSY}}} \right)^2. \quad (22)$$

Acknowledgements

J.P. acknowledges support from the MEC and FEDER (EC) Grants FPA2011–23596 and the Generalitat Valenciana under grant PROMETEOII/2013/017. We also acknowledge support from DFG Grants STO/876/2-1, STO/876/6-1.

A Appendix

In this Appendix we provide the full one-loop results for the muon self energy and the magnetic moment, defined in Eqs. (9, 11). We use the notation of Ref. [33], which is similar to the ones from Refs. [26, 27]. Note that in the standard case

of the MSSM with moderate $\tan\beta \lesssim 50$, the combination $m_\mu \tan\beta$ frequently appears. An important difference is that here we have to take into account the distinction between the tree-level and the physical muon mass, $m_\mu^{\text{tree}} \neq m_\mu$, and we have to use the identification (10),

$$m_\mu^{\text{tree}} \tan\beta = m_\mu \tan\beta^{\text{eff}} = y_\mu v_u = y_\mu \frac{\sqrt{2}M_W}{g_2}, \quad (23)$$

which is exactly valid. Here g_2 denotes the SU(2) gauge coupling.

The relevant interaction terms for chargino–sneutrino and neutralino–smuon interactions with muons can be written as

$$\mathcal{L}_{\text{int}} = \overline{\tilde{\chi}_i^-} \left(c_{i\tilde{\nu}_\mu}^L P_L + c_{i\tilde{\nu}_\mu}^R P_R \right) \mu \tilde{\nu}_\mu^\dagger + \overline{\tilde{\chi}_j^0} \left(n_{j\tilde{\mu}_k}^L P_L + n_{j\tilde{\mu}_k}^R P_R \right) \mu \tilde{\mu}_k^\dagger + \text{h. c.}, \quad (24)$$

where the coupling coefficients are defined as

$$c_{i\tilde{\nu}_\mu}^L = -g_2 V_{i1}^*, \quad (25a)$$

$$c_{i\tilde{\nu}_\mu}^R = y_\mu U_{i2}, \quad (25b)$$

$$n_{j\tilde{\mu}_k}^L = \frac{1}{\sqrt{2}} (g_1 N_{j1}^* + g_2 N_{j2}^*) U_{k1}^{\tilde{\mu}} - y_\mu N_{j3}^* U_{k2}^{\tilde{\mu}}, \quad (25c)$$

$$n_{j\tilde{\mu}_k}^R = -\sqrt{2}g_1 N_{j1} U_{k2}^{\tilde{\mu}} - y_\mu N_{j3} U_{k1}^{\tilde{\mu}}. \quad (25d)$$

The unitary matrices U, V, N diagonalize the chargino and neutralino mass matrices; $U^{\tilde{\mu}}$ is used to diagonalize the smuon mass matrix. The resulting smuon mass eigenvalues are given by

$$m_{\tilde{\mu}_{1/2}}^2 = \frac{1}{2} \left(m_L^2 + m_R^2 + \frac{M_Z^2}{2} \pm \sqrt{\left[m_L^2 - m_R^2 + M_Z^2 \left(\frac{1}{2} - 2s_W^2 \right) \right]^2 + 8y_\mu^2 |\mu|^2 \frac{M_W^2}{g_2^2}} \right). \quad (26)$$

A term containing the trilinear coupling vanishes because of $v_d = 0$, and in the last term we have used Eq. (23). The occurring SUSY parameters are the higgsino mass parameter μ , the gaugino masses M_1 as well as M_2 and the soft mass parameters for the second-generation slepton doublet and singlet m_L and m_R , respectively.

With this notation, the MSSM one-loop contributions to the on-shell muon self-energy from chargino–sneutrino or neutralino–smuon loops can be expressed as $\Sigma_\mu^{\text{MSSM}} = \Sigma_\mu^{\tilde{\chi}^\pm} + \Sigma_\mu^{\tilde{\chi}^0} = -y_\mu v_u \Delta_\mu^{\text{red}}$, with

$$\Sigma_\mu^{\tilde{\chi}^\pm} = \frac{1}{16\pi^2} \sum_i m_{\tilde{\chi}_i^\pm} \text{Re} \left[c_{i\tilde{\nu}_\mu}^L (c_{i\tilde{\nu}_\mu}^R)^* \right] B_0(m_{\tilde{\chi}_i^\pm}, m_{\tilde{\nu}_\mu}), \quad (27a)$$

$$\Sigma_\mu^{\tilde{\chi}^0} = \frac{1}{16\pi^2} \sum_{j,k} m_{\tilde{\chi}_j^0} \text{Re} \left[n_{j\tilde{\mu}_k}^L (n_{j\tilde{\mu}_k}^R)^* \right] B_0(m_{\tilde{\chi}_j^0}, m_{\tilde{\mu}_k}), \quad (27b)$$

where terms suppressed by m_μ/M_{SUSY} or by powers of $\tan\beta$ are neglected. In dimensional regularization with parameter $\epsilon = (4-D)/2$ and regularization scale μ_R , the one-loop integral B_0 is given by

$$B_0(a, b) = \Delta + 1 + \frac{1}{b^2 - a^2} \left(a^2 \ln \frac{a^2}{\mu_R^2} - b^2 \ln \frac{b^2}{\mu_R^2} \right) + \mathcal{O}(\epsilon), \quad (28)$$

with the common quantity

$$\Delta = \frac{1}{\epsilon} + \ln 4\pi - \gamma_E, \quad (29)$$

containing the Euler-Mascheroni constant γ_E . Owing to the unitarity of the mixing matrices, in Eqs. (27) the UV divergences as well as the dependence on μ_R vanish.

Because of $v_d = 0$, the tree-level mass of the muon (as well as the other charged leptons and down-type quarks) equals zero. Therefore, the entire muon mass has to be generated at the loop level, which means

$$m_\mu = -\Sigma_\mu^{\text{MSSM}}. \quad (30)$$

For a given parameter point, this equation can be used to determine the muon Yukawa coupling y_μ . Note that the self energy is approximately linear in y_μ , as suggested by the definition of Δ_μ^{red} in Eq. (9). But the Yukawa coupling also enters nonlinearly, through cubic terms in $n_{j\tilde{\mu}_k}^L (n_{j\tilde{\mu}_k}^R)^*$, and via the smuon masses (26). Therefore, it has to be determined numerically in an exact calculation. As shown in Sec. 2, however, the nonlinear terms vanish in the mass-insertion approximation.

The SUSY one-loop diagrams contributing to the anomalous magnetic moment of the muon are the same as for the muon self-energy, except for the fact that now a photon couples to the charged SUSY particle in the loop, i.e. the chargino or the smuon. Again neglecting terms suppressed by $\tan\beta$, the result reads $a_\mu^{\text{SUSY}} = a_\mu^{\tilde{\chi}^\pm} + a_\mu^{\tilde{\chi}^0} = (y_\mu v_u/m_\mu) a_\mu^{\text{red}}$, with

$$a_\mu^{\tilde{\chi}^\pm} = \frac{m_\mu}{24\pi^2} \sum_i \frac{m_{\tilde{\chi}_i^-}}{m_{\tilde{\nu}_\mu}^2} \text{Re} \left[c_{i\tilde{\nu}_\mu}^L (c_{i\tilde{\nu}_\mu}^R)^* \right] F_2^C(x_i), \quad (31a)$$

$$a_\mu^{\tilde{\chi}^0} = -\frac{m_\mu}{48\pi^2} \sum_{j,k} \frac{m_{\tilde{\chi}_j^0}}{m_{\tilde{\mu}_k}^2} \text{Re} \left[n_{j\tilde{\mu}_k}^L (n_{j\tilde{\mu}_k}^R)^* \right] F_2^N(x_{jk}), \quad (31b)$$

where the mass ratios are given by $x_i = m_{\tilde{\chi}_i^-}^2/m_{\tilde{\nu}_\mu}^2$ and $x_{jk} = m_{\tilde{\chi}_j^0}^2/m_{\tilde{\mu}_k}^2$. The dimensionless loop functions have been introduced in Ref. [26] as

$$F_2^C(x) = \frac{3}{2(1-x)^3} [-3 + 4x - x^2 - 2 \ln x], \quad (32a)$$

$$F_2^N(x) = \frac{3}{(1-x)^3} [1 - x^2 + 2x \ln x], \quad (32b)$$

normalized such that $F_2^C(1) = F_2^N(1) = 1$. The formulas look identical to the respective terms in the standard case with moderate $\tan\beta$, but like for the self energy, there are nonlinear terms in y_μ , which usually are neglected because of the m_μ/M_{SUSY} suppression. In our case, these terms are only suppressed as $M_{W,Z}/M_{\text{SUSY}}$; hence they are much more significant in an exact calculation. Nevertheless, like for the self energy, in the mass-insertion approximation, a_μ^{SUSY} is linear in the Yukawa coupling.

References

- [1] G.W. Bennett *et al.* [Muon ($g-2$) Collaboration], Phys. Rev. D **73**, 072003 (2006).
- [2] R. M. Carey, K. R. Lynch, J. P. Miller, B. L. Roberts, W. M. Morse, Y. K. Semertzides, V. P. Druzhinin and B. I. Khazin *et al.*, FERMILAB-PROPOSAL-0989; B. L. Roberts, Chin. Phys. C **34** (2010) 741 [arXiv:1001.2898 [hep-ex]].
- [3] H. Inuma [J-PARC New $g-2$ /EDM experiment Collaboration], J. Phys. Conf. Ser. **295** (2011) 012032.
- [4] F. Jegerlehner and A. Nyffeler, Phys. Rept. **477** (2009) 1.
- [5] J. Miller, E. de Rafael, B.L. Roberts, D. Stöckinger, Ann.Rev.Nucl.Part. (2012) 62.
- [6] T. Aoyama, M. Hayakawa, T. Kinoshita and M. Nio, Phys. Rev. Lett. **109** (2012) 111808 [arXiv:1205.5370 [hep-ph]].
- [7] A. Kurz, T. Liu, P. Marquard and M. Steinhauser, Nucl. Phys. B **879** (2014) 1 [arXiv:1311.2471 [hep-ph]]. R. Lee, P. Marquard, A. V. Smirnov, V. A. Smirnov and M. Steinhauser, JHEP **1303** (2013) 162 [arXiv:1301.6481 [hep-ph]].
- [8] C. Gnendiger, D. Stöckinger and H. Stöckinger-Kim, Phys. Rev. D **88** (2013) 053005 [arXiv:1306.5546 [hep-ph]].
- [9] M. Davier, A. Hoecker, B. Malaescu and Z. Zhang, Eur. Phys. J. C **71** (2011) 1515 [Erratum-ibid. C **72** (2012) 1874] [arXiv:1010.4180 [hep-ph]].
- [10] K. Hagiwara, R. Liao, A. D. Martin, D. Nomura and T. Teubner, J. Phys. G G **38** (2011) 085003 [arXiv:1105.3149 [hep-ph]].
- [11] M. Benayoun, P. David, L. DelBuono and F. Jegerlehner, arXiv:1210.7184 [hep-ph].

- [12] F. Jegerlehner and R. Szafron, Eur. Phys. J. C **71** (2011) 1632 [arXiv:1101.2872 [hep-ph]].
- [13] A. Kurz, T. Liu, P. Marquard and M. Steinhauser, Phys. Lett. B **734** (2014) 144 [arXiv:1403.6400 [hep-ph]].
- [14] T. Blum, A. Denig, I. Logashenko, E. de Rafael, B. Lee Roberts, T. Teubner and G. Venanzoni, arXiv:1311.2198 [hep-ph].
- [15] M. Benayoun, J. Bijnens, T. Blum, I. Caprini, G. Colangelo, H. Czyz, A. Denig and C. A. Dominguez *et al.*, arXiv:1407.4021 [hep-ph].
- [16] G. Colangelo, M. Hoferichter, B. Kubis, M. Procura and P. Stoffer, Phys. Lett. B **738** (2014) 6 [arXiv:1408.2517 [hep-ph]].
- [17] P. Masjuan, arXiv:1411.6397 [hep-ph].
- [18] A. Czarnecki and W. J. Marciano, Phys. Rev. D **64** (2001) 013014 [hep-ph/0102122].
- [19] F. Borzumati, G. R. Farrar, N. Polonsky and S. D. Thomas, Nucl. Phys. B **555** (1999) 53 [hep-ph/9902443].
- [20] A. Crivellin, J. Girrbach and U. Nierste, Phys. Rev. D **83** (2011) 055009 [arXiv:1010.4485 [hep-ph]].
- [21] A. Thalapillil and S. Thomas, arXiv:1411.7362 [hep-ph].
- [22] M. Carena, M. Olechowski, S. Pokorski and C.E.M. Wagner, Nucl. Phys. **B426** (1994) 269; L.J. Hall, R. Rattazzi and U. Sarid, Phys. Rev. **D50** (1994) 7048; C. Hamzaoui, M. Pospelov and M. Toharia, Phys. Rev. D **59** (1999) 095005; K. S. Babu and C. F. Kolda, Phys. Rev. Lett. **84** (2000) 228; G. Isidori and A. Retico, JHEP **0111** (2001) 001; A. J. Buras, P. H. Chankowski, J. Rosiek and L. Slawianowska, Nucl. Phys. B **659** (2003) 3; T. Blazek, S. Raby and S. Pokorski, Phys. Rev. D **52** (1995) 4151. M. S. Carena, D. Garcia, U. Nierste and C. E. M. Wagner, Nucl. Phys. B **577** (2000) 88 [arXiv:hep-ph/9912516].
- [23] S. Marchetti, S. Mertens, U. Nierste and D. Stöckinger, Phys. Rev. D **79**, 013010 (2009).
- [24] B. A. Dobrescu and P. J. Fox, Eur. Phys. J. C **70** (2010) 263 [arXiv:1001.3147 [hep-ph]].
- [25] W. Altmannshofer and D. M. Straub, JHEP **1009** (2010) 078 [arXiv:1004.1993 [hep-ph]].

- [26] S. P. Martin and J. D. Wells, Phys. Rev. D **64** (2001) 035003 [hep-ph/0103067].
- [27] D. Stöckinger, “The Muon Magnetic Moment and Supersymmetry,” J. Phys. G**34** (2007) R45-R92.
- [28] G.-C. Cho, K. Hagiwara, Y. Matsumoto and D. Nomura, JHEP **1111** (2011) 068 [arXiv:1104.1769 [hep-ph]].
- [29] M. Endo, K. Hamaguchi, S. Iwamoto and T. Yoshinaga, JHEP **1401** (2014) 123 [arXiv:1303.4256 [hep-ph]].
- [30] M. Endo, K. Hamaguchi, T. Kitahara and T. Yoshinaga, JHEP **1311** (2013) 013 [arXiv:1309.3065 [hep-ph]].
- [31] M. Endo, K. Hamaguchi, S. Iwamoto, T. Kitahara and T. Moroi, Phys. Lett. B **728** (2014) 274 [arXiv:1310.4496 [hep-ph]].
- [32] H. G. Fargnoli, C. Gnendiger, S. Paßehr, D. Stöckinger and H. Stöckinger-Kim, Phys. Lett. B **726** (2013) 717 [arXiv:1309.0980 [hep-ph]].
- [33] H. Fargnoli, C. Gnendiger, S. Paßehr, D. Stöckinger and H. Stöckinger-Kim, JHEP **1402** (2014) 070 [arXiv:1311.1775 [hep-ph]].
- [34] J. L. Evans, M. Ibe, S. Shirai and T. T. Yanagida, Phys. Rev. D **85** (2012) 095004 [arXiv:1201.2611 [hep-ph]].
- [35] M. Ibe, S. Matsumoto, T. T. Yanagida and N. Yokozaki, JHEP **1303** (2013) 078 [arXiv:1210.3122 [hep-ph]].
- [36] M. Ibe, T. T. Yanagida and N. Yokozaki, JHEP **1308** (2013) 067 [arXiv:1303.6995 [hep-ph]].
- [37] G. Bhattacharyya, B. Bhattacharjee, T. T. Yanagida and N. Yokozaki, Phys. Lett. B **730** (2014) 231 [arXiv:1311.1906 [hep-ph]].
- [38] S. Mohanty, S. Rao and D. P. Roy, JHEP **1309** (2013) 027 [arXiv:1303.5830 [hep-ph]].
- [39] I. Gogoladze, F. Nasir, Q. Shafi and C. S. Un, Phys. Rev. D **90** (2014) 3, 035008 [arXiv:1403.2337 [hep-ph]].
- [40] M. Badziak, Z. Lalak, M. Lewicki, M. Olechowski and S. Pokorski, arXiv:1411.1450 [hep-ph].
- [41] K. Kowalska, L. Roszkowski, E. M. Sessolo and A. J. Williams, arXiv:1503.08219 [hep-ph].

- [42] F. Wang, W. Wang and J. M. Yang, arXiv:1504.00505 [hep-ph].
- [43] A. Freitas, J. Lykken, S. Kell and S. Westhoff, JHEP **1405** (2014) 145 [Erratum-ibid. **1409** (2014) 155] [arXiv:1402.7065 [hep-ph]].
- [44] S. Heinemeyer, D. Stöckinger and G. Weiglein, Nucl. Phys. B **690** (2004) 62.
- [45] S. Heinemeyer, D. Stöckinger and G. Weiglein, Nucl. Phys. B **699** (2004) 103.
- [46] T. Moroi, Phys. Rev. D **53** (1996) 6565 [Erratum-ibid. D **56** (1997) 4424] [hep-ph/9512396].
- [47] G. Degrassi and G. F. Giudice, Phys. Rev. D **58** (1998) 053007.
- [48] P. Grothaus, M. Lindner and Y. Takanishi, JHEP **1307** (2013) 094 [arXiv:1207.4434 [hep-ph]].
- [49] J. Kersten, J.-h. Park, D. Stöckinger and L. Velasco-Sevilla, JHEP **1408** (2014) 118 [arXiv:1405.2972 [hep-ph]].
- [50] P. von Weitershausen, M. Schäfer, H. Stöckinger-Kim and D. Stöckinger, Phys. Rev. D **81** (2010) 093004.
- [51] J. Hisano and S. Sugiyama, Phys. Lett. B **696** (2011) 92 [Erratum-ibid. B **719** (2013) 472] [arXiv:1011.0260 [hep-ph]].
- [52] T. Kitahara, JHEP **1211** (2012) 021 [arXiv:1208.4792 [hep-ph]].
- [53] M. Carena, S. Gori, I. Low, N. R. Shah and C. E. M. Wagner, JHEP **1302** (2013) 114 [arXiv:1211.6136 [hep-ph]].
- [54] T. Kitahara and T. Yoshinaga, JHEP **1305** (2013) 035 [arXiv:1303.0461 [hep-ph]].
- [55] S. P. Martin, Phys. Rev. D **66** (2002) 096001 [hep-ph/0206136].
- [56] J.-h. Park, JCAP **1102** (2011) 023 [arXiv:1011.4936 [hep-ph]]; Phys. Rev. D **83** (2011) 055015 [arXiv:1011.4939 [hep-ph]].
- [57] M. Graesser and S. D. Thomas, Phys. Rev. D **65** (2002) 075012 [hep-ph/0104254].
- [58] Z. Chacko and G. D. Kribs, Phys. Rev. D **64** (2001) 075015 [hep-ph/0104317].
- [59] G. Isidori, F. Mescia, P. Paradisi and D. Temes, Phys. Rev. D **75** (2007) 115019 [hep-ph/0703035 [HEP-PH]].

- [60] W. C. Chiu, C. Q. Geng and D. Huang, Phys. Rev. D **91** (2015) 1, 013006 [arXiv:1409.4198 [hep-ph]].
- [61] J. Adam *et al.* [MEG Collaboration], Phys. Rev. Lett. **110** (2013) 201801 [arXiv:1303.0754 [hep-ex]].
- [62] Y. Okada, M. Yamaguchi and T. Yanagida, Prog. Theor. Phys. **85** (1991) 1; Phys. Lett. B **262** (1991) 54; J. R. Ellis, G. Ridolfi and F. Zwirner, Phys. Lett. B **257** (1991) 83; Phys. Lett. B **262** (1991) 477; H. E. Haber and R. Hempfling, Phys. Rev. Lett. **66** (1991) 1815.
- [63] A. Brignole, G. Degrassi, P. Slavich and F. Zwirner, Nucl. Phys. B **643** (2002) 79 [hep-ph/0206101].
- [64] J. F. Gunion and H. E. Haber, Phys. Rev. D **67** (2003) 075019 [hep-ph/0207010].
- [65] G. Degrassi, P. Slavich and F. Zwirner, Nucl. Phys. B **611** (2001) 403 [hep-ph/0105096].